Title: STK25 inhibits PKA signaling by phosphorylating PRKAR1A

Authors: Xiaokan Zhang[1], Bryan Z. Wang[1,2], Michael Kim[1], Trevor R. Nash[1,2], Bohao Liu[1,2], Jenny Rao[1], Roberta Lock[2], Manuel Tamargo[2], Rajesh Kumar Soni[3], John Belov[1], Eric Li[1], Gordana Vunjak-Novakovic[1,2] and Barry Fine[1*]

Affiliations

[1] Department of Medicine, Division of Cardiology, Columbia University Irving Medical Center, New York, NY, USA

[2] Department of Biomedical Engineering, Columbia University, New York, NY, USA

[3] Proteomics and Macromolecular Crystallography Shared Resource, Herbert Irving Comprehensive Cancer Center, Columbia University Irving Medical Center, New York, NY, USA

***Corresponding Author**

Barry Fine MD PhD

Department of Medicine, Division of Cardiology

622 West 168th Street

PH8-405B

New York, NY 10032

Keywords: STK25, PRKAR1A, Protein Kinase A, induced pluripotent stem cell

Summary

In the heart, Protein Kinase A (PKA) is critical for activating calcium handling and sarcomeric proteins in response to beta adrenergic stimulation leading to increased myocardial contractility and performance. The catalytic activity of PKA is tightly regulated by regulatory subunits which inhibit the catalytic subunit until released by cAMP binding. Phosphorylation of Type II regulatory subunits promotes PKA activation, however the role of phosphorylation in Type I regulatory subunits remain uncertain. Here we utilized human induced pluripotent stem cell cardiomyocytes (iPSC-CM) to identify STK25 as a kinase of the Type Iα regulatory subunit PRKAR1A. Phosphorylation PRKAR1A led to inhibition of PKA kinase activity and increased binding to the catalytic subunit in the presence of cAMP. *Stk25* knockout in mice diminished Prkar1a phosphorylation, increased Pka activity and augmented contractile response to beta adrenergic stimulation. Together, these data support STK25 as a negative regulator of PKA signaling through phosphorylation of PRKAR1A.

Introduction

Second messengers are key relays in the transduction of external cues into intracellular signaling cascades. cAMP is a prototypical second messenger generated downstream from G protein coupled receptors and is involved in integrating a diverse set of signaling pathways (1). The classic and most widely studied effector of cAMP is PKA and it has been broadly implicated in a diverse set of cellular processes including the cell cycle, proliferation, cytoskeletal dynamics, ion flux and beta adrenergic signaling (2, 3). Specificity of signaling in a system with such a broad set of substrates relies on careful regulation of both cAMP metabolism as well as compartmentalization of PKA through a series of A kinase anchoring proteins (AKAP) (4). These AKAPs bind to the regulatory subunits of PKA and direct its activity to a discrete set of effectors and substrates, thereby allowing for enhanced spatiotemporal control over PKA and the pathways it activates.

The PKA holoenzyme is comprised of a regulatory subunit dimer and two catalytic units (5). The main function of the regulatory subunit is to inactivate kinase activity in the absence of cAMP. There are two classes of regulatory subunits, Type I and Type II, each with an alpha and beta isoform. Binding of cAMP to the C terminal tandem cAMP binding domains of the regulatory subunits releases the catalytic domain, allowing for kinase activity (6). Type II regulatory subunits have a PKA substrate motif in the N -terminus (RRXS), which is phosphorylated by the catalytic subunit upon binding to cAMP, enhancing its release and activation (7). They also are the primary target of AKAPs, binding at nanomolar affinities (4). The regulation of Type I subunits however remains less well understood. They contain a pseudo-substrate (RRXxA/G) sequence that cannot be phosphorylated by the catalytic subunit. Although phosphorylation of the Type I subunits has been reported as part of large phosphoproteomic projects, their role in *in vivo* regulation of PKA activity has not been demonstrated (8-12). Furthermore, the vast majority AKAP proteins do not interact with Type I subunits, and the dual specificity AKAP proteins that do interact with Type I subunits do so with significantly lower affinities compared to Type II subunits.

In the heart, PKA mediates beta adrenergic activation of the physiologic flight or fight response, modulating both heart rate and myocardial contractility (13). Substrates of PKA in the cardiomyocyte include troponin (TNNT2), myosin binding protein c (MYBPC3), phospholamban (PLN), and ryanodine receptor (RYR2) (14). Acute activation of PKA in hyperadrenergic states leads to improved calcium flux and myocardial performance and is necessary for increases in stroke volume to meet cardiac output demands. In heart failure, chronic beta-adrenergic stimulation from high levels of catecholamines results in compensatory downregulation of beta adrenergic signaling leading diminished phosphorylation of several PKA substrates (15, 16). Long term activation of Pka was shown to be deleterious in mouse models and is thought to underly the maladaptive remodeling of chronic beta adrenergic activation in heart failure (17). In one proposed model, hyperphosphorylation of Ryr2 by PKA leads to depletion of calstabin and leakage of calcium from the sarcoplasmic reticulum during diastole (18). This loss of calcium stores from the sarcoplasmic reticulum contributes to a reduction in contractility in heart failure and arrhythmias due to delayed after depolarizations from inward current (19). This mechanism however is controversial as several other mouse models of Ryr2 hyperphosphorylation have not recapitulated the same phenotype (20, 21).

STK25 is a stress response kinase in the sterile-20 (Ste20) kinase superfamily and has been shown through a series of *in vivo* models to impact glucose utilization, insulin homeostasis, and lipid metabolism (22-30). Overexpression of STK25 leads to steatosis and was shown to aggravate atherosclerosis in a PCSK9 gain of function mouse model (31). Recently, STK25 was shown to interact with the Hippo signaling via phosphorylation of LATS1/2 and/or regulation of SAV1-STRIPAK (32, 33). In this study, we use a combination of *in vitro* and *in vivo* cardiomyocytes models to demonstrate that STK25 phosphorylates the Type Iα regulatory subunit of PKA, PRKAR1A. This leads to increased inhibition of PKA signaling revealing a new regulatory mechanism that can control PKA activity and attenuate cAMP mediated increases in cardiac contractile function.

Methods:

Patient samples

Patients with advanced HF were recruited at Columbia University Medical Center and heart tissue at the time of heart transplant was collected from the left ventricle. Control myocardial samples were obtained from the National Disease Research Interchange (https://ndriresource.org/ats) and was comprised of de-identified specimens collected from non-failing hearts determined to be unusable for cardiac transplantation due to non-cardiac donor issues but without evidence or knowledge of underlying cardiac disease. The study was approved by the Institutional Review Board of Columbia University (IRB# AAAR0055). All patients provided written informed consent before inclusion into the study.

Cell culture

HEK293T cells (ATCC Cat# CRL-3216, RRID:CVCL_0063) were cultured in high glucose (4.5g/L) DMEM supplemented with 10% FBS, penicillin and streptomycin, and grown in a CO_2 incubator maintained at atmospheric oxygen levels and 5% CO_2.

Human induced pluripotent stem cells (hiPSC) were obtained through Material Transfer Agreements from Bruce Conklin, Gladstone Institute (WTC cell line). hiPSCs were expanded on growth factor reduced Matrigel-coated plates (Corning) in mTeSR plus medium (Stemcell technologies) containing mTeSR plus supplement (Stemcell technologies), 50U penicillin and 50U streptomycin. The cell culture medium was changed every other day, and cell passaged upon reaching 70% confluence. During the first 24 hrs after passaging, 5 μM Y-27632 dihydrochloride (Tocris, 1254) was supplemented to culture medium.

CRISPR-Cas9

CRISPR-Cas9 Genome editing was used to generate a homozygous knockout of STK25 in WTC iPSCs following the manufacturer's protocol (ORIGENE) with gRNA vector (KN203215G).

Single-cell clones were expanded and confirmation of homozygous editing was determined by sanger sequencing of gDNA and protein analysis by western blot.

iPS Cardiomyocyte Differentiation

Cardiac differentiation of iPSC's was initiated in confluent monolayers two days after replating at a density of 200,000/cm^2 (24hrs in mTeSR plus medium with 5μM Y-27632 dihydrochloride, followed by 24hrs in mTeSR plus medium without Y-27632). On day 0 of differentiation, media was changed to cardiac differentiation medium (CDM, consisting of RPMI-1640 (Life Technologies), 500μg/ml human recombinant albumin (Sigma), 213μg/ml L-ascorbic acid (Sigma), 50U penicillin and 50U streptomycin) with 3-6 μM CHIR (4423, Tocris). 2 days after initial CHIR addition, media was changed to CDM with 2 μM Wnt-C59 (5148, Tocris). From day 4 onwards, media was changed fresh CDM every other day until cells start contracting. Media was then switched to RPMI-B27 (consisting of RPMI-1640, 1x B27 supplement (Life Technologies), 213μg/mL L-ascorbic acid, 50U penicillin and 50U streptomycin). Cardiomyocytes were characterized by flow cytometry using the cardiomyocyte-specific marker TNNT2 (BD Biosciences Cat# 565744, RRID:AB_2739341). Differentiation typically resulted in cell populations containing 80–90% TNNT2-positive cells at day 12.

PKA activity assay

PKA activity assay was performed using whole cell lysate from iPSC-CMs treated with either PBS or 10μM forskolin (Sigma-Aldrich, F6886) for 30min at 37°C prior to assay, or whole heart lysates from Stk25$^{+/+}$ or Stk25$^{-/-}$ mice following the manufacturer's protocol (EIAPKA, Invitrogen). Briefly, PKA standards or diluted samples and reconstituted ATP were added into wells of PKA substrate plate. Phospho-PKA substrate antibody and Goat anti-Rabbit IgG HRP conjugate antibody were added into the wells per manufacturer protocol. After incubation TMB substrate was added into

each well, and the plate was incubated for 30 min at room temperature. Stop solution was added, and absorbance at 450nm was analyzed in a 96-plate reader.

Global Phosphoproteomics analysis

Sorted WTC and STK25-/- iPSC-CMs were lysed/homogenized by bead-beating in 8 M urea/1%SDS and 200 mM EPPS (pH 8.5), protease, and phosphatase inhibitors. Lysates were cleared by centrifugation at 21,000 g for 30 min at 4^0C, and protein concentration was measured by BCA. Proteins were reduced with 5 mM TCEP, alkylated with 10 mM iodoacetamide (IAA), and quenched with 10 mM DTT. A total of 500 µg of protein was chloroform−methanol precipitated. Protein was reconstituted in 200 mM EPPS (pH 8.5) and digested by Lys-C overnight and trypsin for 6 h, both at a 1:50 protease-to-peptide ratio. Digested peptides were quantified using a Nanodrop at 280 nm, and 200 µg of peptide from each sample were labeled with 800 µg TMT reagent using a 10-plex TMT kit (34). TMT labels were checked, 100 ng of each sample was pooled and desalted and analyzed by short SPS-MS3 method, and using normalization factor samples were bulk mixed at 1:1 across all channels and desalted using a 200 mg Sep-Pak solid-phase extraction column and dried using vacuum centrifugation.

Desalted isobaric labeled peptides were enriched for phospho-peptides using a mixture of MagReSyn Ti-IMAC and Zr-IMAC resins according ReSyn Bioscience instructions. In brief, 1.4 mg of labeled peptide were resuspended in 1 ml of binding buffer (80% Acetonitrile, 1M glycolic acid and 5% TFA) and incubated with equilibrated 150 µl (75 µl of each Ti-IMAC and Zr-IMAC) resins at room temperature for 30 min, and the resin was washed 3 three times to remove the unbound, non-phosphorylated peptides. Phospho-peptides were eluted using 1% ammonium hydroxide. The enriched phospho-peptides were further fractionated in eight fractions using Pierce™ High pH Reversed-Phase Peptide Fractionation Kit and each fraction dried down in a speed-vac.

The isobaric labeled dried phospho-peptides were resuspended in 10 µl of (3% acetonitrile/ 0.1% formic acid), and analyzed on an Orbitrap Fusion mass spectrometer coupled to a Dionex Ultimate 3000 (ThermoFisher Scientific) using the MSA-SPS-MS3 and NL SPS-MS3 method (35). Peptides were separated on an EASY-Spray C18 50cm column (Thermo Scientific). Peptide elution and separation were achieved at a non-linear flow rate of 250 nl/min using a gradient of 5-30% of buffer B (0.1% (v/v) formic acid, 100% acetonitrile) for 110 minutes with a temperature of the column maintained at 50 °C during the entire experiment. For both methods, MS1 data were collected using the Orbitrap (120,000 resolution; maximum injection time 50 ms; AGC 4×10^5). Determined charge states between 2 and 5 were required for sequencing and a 45 s dynamic exclusion window was used. Data-dependent top10 MS2 scans were performed in the ion trap with collision-induced dissociation (CID) fragmentation (Turbo; NCE 35%; maximum injection time 60ms; AGC 5×10^4). MS3 quantification scans were performed using the multi-notch MS3-based TMT method (ten SPS ions; 50,000 resolution; NCE 65% for MSA-SPS-TMT and 38% for NL-SPS-TMT maximum injection time 105 ms; AGC $1x10^5$) using the Orbitrap.

Raw mass spectrometric data were analyzed using Proteome Discoverer 2.2 to perform database search and TMT reporter ions quantification. TMT tags on lysine residues and peptide N termini (+229.163 Da) and the carbamidomethylation of cysteine residues (+57.021 Da) was set as static modifications, while the oxidation of methionine residues (+15.995 Da), deamidation (+0.984) on asparagine and glutamine and phosphorylation (+79.966) on serine, threonine, and tyrosine were set as a variable modification. Data were searched against a UniProt Human database with peptide-spectrum match (PSMs) and protein-level FDR at 1% FDR. The signal-to-noise (S/N) measurements of each protein normalized so that the sum of the signal for all proteins in each channel was equivalent to account for equal protein loading. Phospho-peptides identification and quantification were imported into Perseus (36) for t-test statistical analysis (FDR<0.05) to identify phospho-peptides demonstrating statistically

significant changes in abundance. Pathway analysis were performed using Ingenuity Pathway Analysis (Qiagen).

Animal studies

Stk25 knockout mice were generated by CRISPR/Cas9 mediated genome engineering in C57BL/6J background (Jackson Laboratory, Bar Harbor, Maine). Exon 3-5 of Stk25 gene were deleted with two CRISPR guides from Synthego (sgRNA-stk25-7367 and sgRNA-stk25-10150). Both guides were mixed with IDT Cas9V3 protein to form RNP, which was further injected into the pronuclei of fertilized C57BL/6J eggs to generate knockout founders. Genotyping was performed to show the *Stk25* knockout allele. Further breeding generated homozygous *Stk25*$^{-/-}$ mice and protein immunoblotting was performed to confirm an absence of Stk25. The protocol for all mouse experiments (AABC1503) was approved by the Columbia University Institutional Animal Care and Use Committee.

Cardiac function of 20 week and 52 week old mice was assessed by echocardiography by the Columbia University Mouse Imaging Core Facility (imaged by Visulasonics VEVO 3100 High Frequency Ultrasound imaging system and analyzed by Vevo LAB software). Cardiac function was recorded at baseline and after administration of the β-adrenergic receptor agonist isoproterenol (0.2ug/g, i.p.). Systolic function parameters including ejection fraction (EF, %), fractional shortening (FS, %), left ventricular end systolic diameter (LVESD, mm) and left ventricular end diastolic diameter (LVEDD, mm) were measured in the two-dimensional parasternal short-axis imaging plane of M-mode tracings close to the papillary muscle level. For isoproterenol studies, the ratio of each parameter value after the injection of isoproterenol was compared to the pre-injection parameter value and the response was calculated for each individual heart as a ratio of the two.

iPS Cardiomyocyte sorting

Cardiomyocytes were pretreated with 10μM of Y-27632 in B27 culture medium for 6 hrs, then digested with cell dissociation buffer (containing Hank's buffered saline solution, 100 Units/ml collagenase, 10μM Y-27632) at room temperature overnight. Cells were collected and centrifuged at 300g for 5 min, and then resuspended in cell sorting buffer (CSB, containing Hank's buffered saline solution, 20mM HEPES, 5% FBS, 10 units/ml Turbo DNase). The cell pellet was resuspended with anti-CD172a/b (SIRPα/β, 423107, Biolegend) and anti-CD90 (Thy-1, 11-0909-42, Invitrogen) antibodies in CSB to stain for 20 min at 4°C in the dark. Cells were washed 3 times with CSB and DAPI staining was added. Cardiomyocytes were sorted from the SIRPA+ and CD90- population and then plated on matrigel coated plates in B27 medium with 5μM Y-27632. The following day, medium was replaced with fresh B27, and cardiomyocytes generally started to beat in 2-5 days.

RNA Isolation, Sequencing, and Analysis.

RNA was extracted using the RNeasy Mini kit (Qiagen #74004) along with on-column DNAse digestion (Qiagen #79254). cDNA libraries were generated using the Clontech Ultra Low v4 kit followed by NextaraXT DNA Library Prep Kit, then sequenced on an Illumina NovaSeq 6000. Paired-end 100-bp sequenced reads were analyzed as follows: RTA (Illumina) software was used for base calling and bcl2fastq2 (version 2.19) for converting BCL to fastq format, coupled with adaptor trimming. A pseudoalignment to a kallisto index created from transcriptomes (build GRCh38) using kallisto (0.44.0). After pseudoalignment the R package DESeq2 (1.28.1) was used to normalize the count matrix and calculate differentially expressed genes. Geneset enrichment analysis was performed using GSEA software (4.10.0) per documentation (37, 38).

siRNA and vector transfection

Cells were transfected using lipofectamine 3000 (Invitrogen) following the manufacturer's protocol with siRNA targeting STK25 (On-TargetPlus siRNA, Horizon Discovery, L-004873-00-0050) or siRNA targeting PRKAR1A (EHU071341, Sigma) for protein knockdown or non-targeting control siRNA (ON-TARGETplus non-targeting pool, Horizon Discovery D-001810-10-50) as scramble control.

For heterologous expression studies, cells were transfected using lipofectamine 3000 (Invitrogen, L3000015) following the manufacturer's protocol. Vectors used include Flag-WT-STK25 vector (EX-M0142-M46, GeneCopoeia), Flag-K49R/T147A-STK25 vector (Vector Builder), Flag- empty vector (EX-NEG-M46, GeneCopoeia), V5-PRKAR1A (Vector Builder, VB200124-1141aes), V5-S77A/S83A-PRKAR1A (Vector Builder, VB200124-1126jtp), and V5-S77E/S83E-PRKAR1A (Vector Builder, VB200124-1127pst).

qRT-PCR assays

Equivalent amounts (2µg) of purified RNA were used as a template to synthesize cDNA using oligo-d(T) primers and SuperScript™ III First-Strand Synthesis SuperMix (Invitrogen, 18080400). *STK25* was quantified by real-time PCR using Fast SYBR Green mixture (Life Technologies, 4385612) and was carried out on Applied Biosystems Step One Plus. Relative levels were calculated using ΔΔCт method. Data analysis was carried out using the fold change normalized to GAPDH gene expression.

Gene	Forward Primer 5'-3'	Reverse Primer 5'-3'
STK25	GCTCCTACCTAAAGAGCACCA	TGGCAATGTATGTCTCCTCCAG
GAPDH	GGACTCATGACCACAGTCCATG	CAGGGATGATGTTCTGGAGAGC

Immunoprecipitation and immunoblot analysis

300 µg of total protein from whole cell lysate were used in immunoprecipitation. The extract was incubated with anti-Flag affinity gel (Sigma-Aldrich Cat# A2220, RRID:AB_10063035) or anti-V5 affinity gel (Sigma-Aldrich Cat# A7345, RRID:AB_10062721) overnight at 4°C. The affinity gel

beads were centrifuged at 8000xg for 1min, washed three times in TBS buffer. The affinity gel beads were added with 4x Laemmli SDS sample buffer (NuPAGE), denatured at for 5min at 95°C and analyzed by SDS-PAGE and immunoblotting. For Western blotting antibodies include: HRP conjugated anti-GAPDH (Cell Signaling Technology Cat# 3683, RRID:AB_1642205), anti-STK25 (Abcam Cat# ab157188, RRID:AB_2725788), anti-Flag (Sigma-Aldrich Cat# F3165, RRID:AB_259529), anti-GM130 (Cell Signaling Technology Cat# 12480, RRID:AB_2797933), anti- PRKAR1A (Abcam Cat# ab139695, RRID:AB_2893184), anti-pS77 PRKAR1A (Abcam Cat#ab139682, RRID:AB_2904566), anti-pS83 PRKAR1A (Abcam Cat#ab154851, RRID:AB_2904567), anti-phospholamban (Cell Signaling Technology Cat# 14562, RRID:AB_2798511), anti-phospho-phospholamban -S16/T17 (Cell Signaling Technology Cat# 8496, RRID:AB_10949102), anti-Ryanodine receptor 2 (Abcam Cat#ab196355, RRID:AB_2904568), anti-p- Ryanodine receptor 2-S2808 (Abcam Cat# ab59225, RRID:AB_946327), anti-V5 (Sigma-Aldrich Cat# V8137, RRID:AB_261889), anti-PKA Catalytic subunit (Abcam Cat# ab26322, RRID:AB_2170049), HRP-conjugated anti-mouse (Cell Signaling Technology Cat# 7076, RRID:AB_330924) and HRP-conjugated anti-rabbit (Cell Signaling Technology Cat# 7074, RRID:AB_2099233) were used for detection.

In vitro kinase assay

Recombinant protein STK25 (500ng, TP303215, OriGene) and PRKAR1A (500ng, H00005573_P01, Abnova) were mixed with in vitro kinase buffer (9802, Cell Signaling) containing ATP (100uM) and incubated at 37°C for 15min. In vitro kinase assay was terminated by adding Laemmli SDS sample buffer. Phosphorylation level of PRKAR1A was analyzed by SDS-PAGE and immunoblotting.

Real Time Glo cell viability assay

Cells were seeded into 96-well plates at a density of 3000 cells per well 24h before measurement. RealTime-Glo (Promega; G9712) reagent was added to each well per manufacturer protocol and measurement of luminescence was performed at selected time points on a BioTek Synergy JHTX with Gen5 data analysis software.

Statistical Analysis:

Statistical analyses were performed using Prism 8 (Graphpad Software). Results are presented as mean ± standard deviation. For comparisons between two groups, a two tailed unpaired t-test was used unless otherwise specific. Welch's correction was utilized for two groups of unequal sizes. For multiple group comparisons, either one way or two-way (depending on the number of variables) ANOVA followed by Tukey's post-hoc test was performed using Prism 8. Notation in the text is as follows *p<0.05, **p<0.01, ***p<0.001 and ****p<0.0001

Results:

STK25 inhibits PKA signaling.

As part of an kinome knockout discovery project, CRISPR-Cas9 was used to generate a homozygous knockout of *STK25* in the wild type iPSC line WTC11 (Bruce Conklin, Gladstone Institute) (39), and cardiomyocytes were differentiated and characterized using an established protocol (40). Since STK25 had not been studied in cardiomyocytes previously, we investigated potential substrates of STK25 and impacted signaling pathways in iPSC-CM using global phosphoproteomics. Ingenuity Pathway Analysis (Qiagen) was performed on differential phosphorylated residues obtained with mass spectrometry in $STK25^{-/-}$ and isogenic $STK25^{+/+}$ iPSC-CMs (**Figure 1A**). A decrease in Hippo signaling was observed in response to loss of STK25 (**Figure 1B**) confirms a prior report indicating STK25 as an activator of Hippo pathway (32). The largest signaling change in response to loss of STK25 was an upregulation of the PKA

pathway. Several downstream substrates of PKA displayed increased phosphorylation including MYBPC3, TNNT2, RYR2, CACNA1C and GSK3α (**Table 1**). *STK25*$^{-/-}$ cardiomyocytes exhibited increased PKA activity when stimulated with the adenylate cyclase agonist forskolin (**Figure 1C**). In heterologous overexpression studies in HEK293T cells, STK25 decreased forskolin induced PKA activity. This inhibition was dependent on the kinase domain of STK25 as overexpression of the kinase dead mutant *STK25*$^{K49R/T174A}$ (41) did not inhibit PKA activity in response to forskolin (**Figure 1D)**.

STK25 phosphorylates PRKAR1A

Two of the most downregulated phosphorylation sites in STK25$^{-/-}$ iPSC-CM were S77 and S83 of PRKAR1A raising the possibility that these sites were directly phosphorylated by STK25 (**Table 1**) (42). We first confirmed the phosphoproteomic data by demonstrating decreased phosphorylation of S77 and S83 in *STK25*$^{-/-}$ cardiomyocytes by immunoblot protein analysis (**Figure 2A**). In order to determine if this observation was dependent on the kinase activity of STK25, STK25$^{K49R/T174A}$ was expressed in *STK25*$^{-/-}$ iPSC-CMs and did not result in an increase in phosphorylation of S77 and S83 as observed in overexpression of wild type STK25 (**Figure 2B**). Stimulation of PKA with forskolin led to diminished phosphorylation at both S77 and S83 in *STK25*$^{+/+}$ to approximately a similar level to unstimulated *STK25*$^{-/-}$ iPSC-CMs (**Figure 2C**).

Co-immunoprecipitations experiments demonstrated STK25 and PRKAR1A binding using epitope tagged protein in HEK293T cells (**Figure 2D**). Though forskolin inhibited binding between PRKAR1A and PRKACA, it did not appear to alter the association between STK25 and PRKAR1A (**Figure 2E**). Mutation of the kinase domain of STK25 also did not affect binding to PRKAR1A (**Figure S1A**). Using purified protein in an *in vitro* kinase assay, STK25 was able to phosphorylate PRKAR1A at S83; however, we were unable to detect direct phosphorylation at S77 (**Figure 2F and data not shown**). This suggests either that STK25 promotes the phosphorylation of S77 indirectly or a yet unidentified cofactor is required for STK25 phosphorylation at that site.

Phosphorylation of S77/S83 inhibits PKA activity

Phosphorylation at S77 and S83 on PRKAR1A have been described as part of large scale global phosphoproteomic experiments (8-10, 43) but their influence on PKA activity has not been characterized. In order to investigate the effect of pS77 and pS83 on the ability of PRKAR1A to inhibit PKA activity, phosphomimetic (*S77E/S83E*) and non-phosphomimetic (*S77A/S83A*) mutations were generated in PRKAR1A expression vectors. In HEK293T co-immunoprecipitation experiments, all three isoforms bind PRKACA similarly (**Figure S1B**). However, upon stimulation with forskolin the S77E/S83E mutant exhibited elevated binding to the catalytic subunit compared to the S77A/S83A and WT PRKAR1A, indicating that positive charges at this residue may interfere with release of PKA in response to cAMP (**Figure 3A)**. We then further tested this hypothesis by assessing PKA kinase activity *in vitro* in response to overexpression of these constructs in HEK293T cells. Though both WT and S77A/S83A PRKAR1A were able to impede forskolin induced PKA activity, expression of the S77E/S83E mutant exhibited no increase in PKA activity in response to forskolin (**Figure 3B**). Similarly, S77E/S83E PRKAR1A was able to inhibit metabolic activity of HEK293T in in response to forskolin (**Figure 3C)** and in normal growth conditions (**Figure S1C)** to a significantly greater degree than either PRKAR1A or STK25 overexpression alone. In order to confirm that PRKAR1A is downstream of STK25, STK25 was overexpressed simultaneously with knock-down of PRKAR1A resulting in rescue of STK25 inhibition of PKA activity (**Figure 3D and Figure S1D**). Together these data demonstrate a new regulatory event where STK25 phosphorylation increased the ability of PRKAR1A bind to the catalytic subunit and inhibit PKA activity in response to cAMP **(Figure 3E)**.

Stk25* loss increases PKA activity *in vivo

In order to validate the STK25-PKA relationship *in vivo*, we generated an *Stk25*$^{-/-}$ mouse and investigated the impact of *Stk25* loss on beta adrenergic stimulation of contraction which is a physiological response mediated by cAMP and PKA. Protein analysis demonstrated that loss of

Stk25 was accompanied by an increase in Prkar1a levels and a significant decrease in the ratio of pS77 and pS83 to total Prkar1a (**Figure 4A and 4B**). Whole heart lysates of *Stk25*$^{-/-}$ mice displayed increased levels of Pka activity compared to wildtype littermates (**Figure 4C**). Downstream targets of Pka including Ryr2 and Pln also exhibited increased phosphorylation (**Figure S2A**).

Since PKA mediates beta adrenergic stimulation of cardiomyocyte contraction function *in* vivo, we assessed the impact of *Stk25* loss on cardiac function in response to the β1 agonist isoproterenol stimulation using echocardiography. Baseline parameters of both LV function and size by echo as well as heart weight to body weight ratio were not different between genotypes and hearts histologically appeared similar without any fibrosis (**Figure S2b, S2c and S2d**). In response to isoproterenol, *Stk25*$^{-/-}$ mice displayed statistically greater individual increases EF and FS (**Figure 4D, 4E and S3a)** and non-statistically significant trends towards decreasing LVESD and LVEDD when compared to *Stk25*$^{+/+}$ mice (**Figures S3b**).

Because prolonged Pka activation has been associated with heart failure (17, 44), a survival cohort of mice at 52 weeks were evaluated by echocardiography and no significant differences in either heart function or left ventricular size were found (**Figure S4**). We then investigated human heart failure samples and found that *STK25* expression was broadly increased in myocardial samples from patients with end stage heart failure when compared to normal heart samples (**Figure 4F and Table S1)**. Using available protein samples from this heart failure cohort, we analyzed the phosphorylation status of PRKAR1A and observed a concordant increase in STK25, PRKAR1A and phosphorylated PRKAR1A (**Figure 4F)**. This raised the possibility that upregulation of STK25 and PRKAR1A has a role in heart failure that may be involved in the downregulation of beta adrenergic signaling.

Discussion

Kinases are integral components of signal transduction pathways, playing key roles in most cellular processes that are initiated by external cues. Therapeutic modulation of kinases has demonstrated success in many branches of medicine, highlighted especially by those that leverage inhibition of kinase cascades implicated in oncogenic processes. Within cardiovascular biology, kinases regulate ion handling, contractility, and metabolism, and their dysregulation is involved in many cardiovascular diseases (45-47). Several kinases including protein kinase A (PKA), Ca2+ calmodulin dependent kinase (CaMK), protein kinase C (PKC) and PIP3 kinase (PI3K) have all been implicated in both physiologic and pathologic signaling (48). Despite this progress, kinase directed therapy has not been developed successfully for cardiovascular diseases, and identifying new regulators of kinase pathways is an area of unrealized therapeutic potential.

Here we present evidence that STK25 is an inhibitor of the PKA pathway, whose phosphorylation of a regulatory subunit drives inhibition of the catalytic subunit's kinase activity. Though phosphorylation of the Type II regulatory subunits has been described in detail, little is known about phosphorylation of Type I regulatory subunits. Phosphorylation at S103 *in vitro* has been shown to be mediated by PKG and interferes potentially with binding to PRKACA (49). Phosphorylation at S83 has been shown to modulate PRKAR1A's association with the replication factor c complex *in vitro*, the consequence of which is unknown (50). In the model we propose, phosphorylation at S77 and S83 increases affinity of PRKAR1A for the catalytic subunit and inhibits cAMP mediated PKA activity. This stands in contrast to the regulation of Type II subunits whose phosphorylation promotes release of the catalytic subunit and thus enhances PKA activity.

Though chronic PKA activation has been associated with progression of heart failure in animal models (14), knockout of *Stk25* resulted in an increase in PKA activity without evidence of heart failure. This discrepancy merits discussion. First it should be noted that mouse models of overexpression of the catalytic PKA subunit resulting in heart failure generate up to 8-fold increases in PKA activity while in our model, mice experience approximately a 1.6-fold increase

in PKA activity. This is in range of prior work demonstrating no heart failure phenotype with *Prkar1a* heterozygosity despite an increase in PKA activity by approximately 1.4-fold. Furthermore, data from human heart failure samples demonstrate *decreased* phosphorylation of PKA targets (51) as chronic hyperstimulation of the beta-adrenergic receptor leads to desensitization and what is thought to be decreased PKA substrate activation (52). We observe *increased* levels of STK25 and phosphorylated PRKAR1A in heart failure samples. This would translate into suppression of PKA stimulation yet it remains to be seen whether these changes are protective (as part of a downregulation response to hyperadrenergic state of heart failure) versus maladaptive (e.g. higher levels of STK25 lead to worsening cardiac performance) or both. While, differences in either heart function or mortality are not observed with loss of *Stk25*, further longitudinal studies with overlayed chronic heart failure models are needed to determine if sustained STK25 loss is a potential therapeutic to improve cardiac function safely.

How exactly phosphorylation of PRKAR1A alters its ability to inhibit the catalytic subunits remains unclear. We observe increased binding of S77E/S83E to the catalytic subunits in forskolin stimulated cells which implies there is either increased affinity between PRKAR1A and the catalytic subunit versus decreased affinity for cAMP by phosphorylated PRKAR1A. Another possibility is a change in PRKAR1A's affinity for an AKAP. Though Type I regulatory subunits generally have weak affinities for AKAP proteins and display a diffuse cytoplasmic localization, the impact that phosphorylation on the assembly of a larger macromolecular regulatory complex remains to be investigated. This is particularly relevant since forskolin did not inhibit PRKAR1A and STK25 binding, yet PRKAR1A phosphorylation was diminished. This would imply that there is either inhibition of STK25 kinase activity by cAMP or a phosphatase that acts on PRKAR1A that is stimulated by cAMP.

In summary, loss of *STK25* leads to increased PKA activity *in vitro* and *in vivo*. We identify PRKAR1A as a new substrate for STK25 and demonstrate that phosphorylation of PRKAR1A at S77 and S83 inhibits PKA signaling. Loss of Stk25 leads to increased physiologic response to

beta adrenergic stimulation of cardiac function without evidence of heart failure. Both STK25 and the phosphorylation of PRKAR1A are upregulated in heart failure and potentially represent a new pathway for downregulation of beta adrenergic signaling in the heart.

Acknowledgements

We would like to thank the Qing Li for his surgical expertise, Erin Bush at the Columbia Genome Center for RNA-seq help, Christopher Damoci at the Columbia Mouse Imaging Core Facility and the labs of Veli Topkara, Elain Wan and Emily Tsai for reagents, technical expertise and tissue samples. B.F is supported by a grant from the NHLBI (K08HL140201), the Gerstner Foundation and the Schwartz Foundation. G.V.N is supported by grants from the NIH (UH3EB025765, P41EB027062, and R01HL076485) and NSF (NSF16478). B.W. T.N and B.L are supported by the MSTP Training Program (T32GM007367). B.L. is also supported by the NIH (F30HL145921). R.K.S is supported by 2P30 CA013696-45 Cancer Center Support Grant.

Competing Interests: None

Data Availability.

RNA-seq data has been deposited in the Gene Expression Omnibus, NCBI: GSE195514

Material Availability

All unique reagents generated in this study are available from the lead contact with a completed materials transfer agreement.

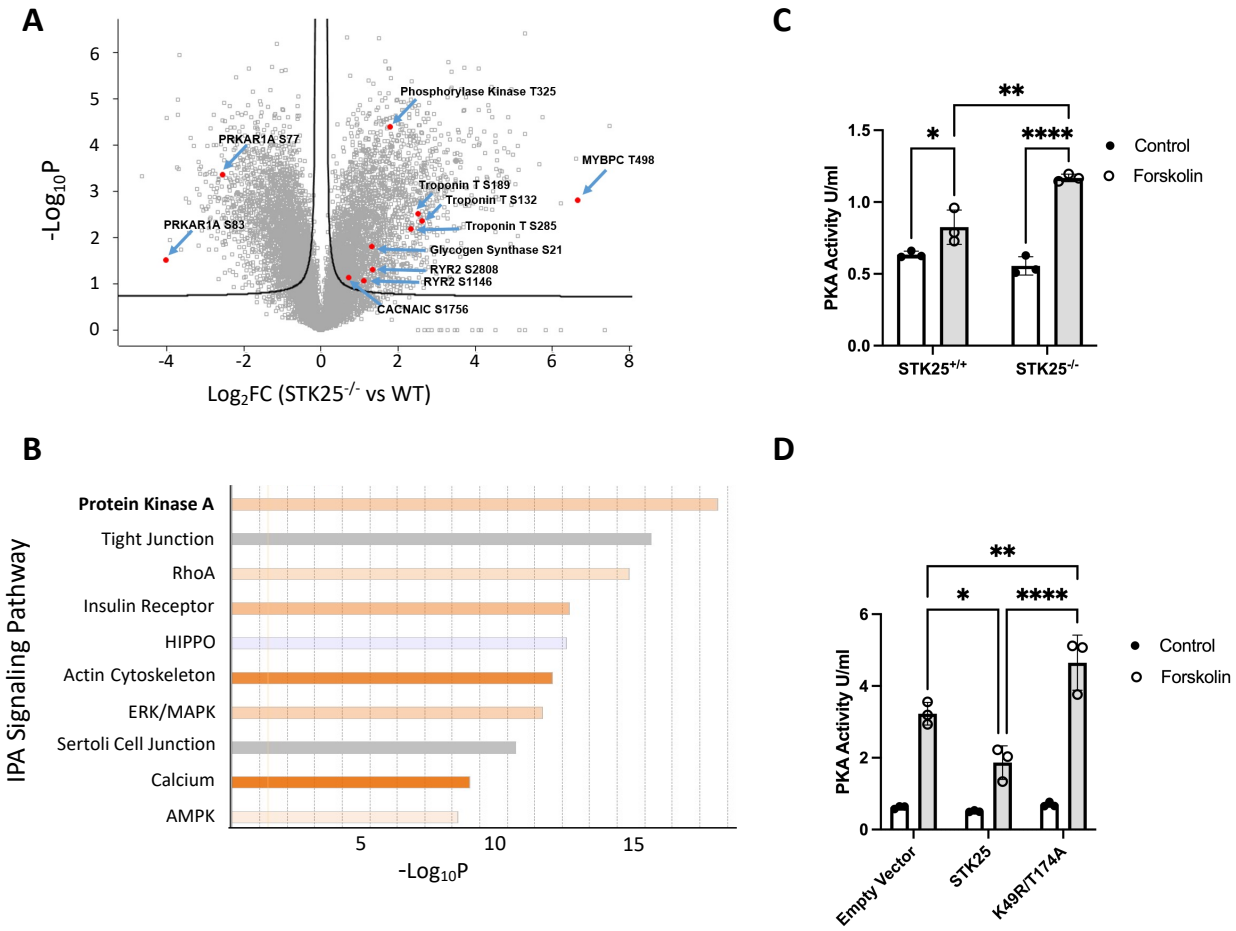

Figure 1. *STK25 inhibits PKA activity.* A) Differential phosphoproteomic spectra of *STK25*$^{+/+}$ and *STK25*$^{-/-}$ cardiomyocytes. Members of the PKA signaling pathway are highlighted. B) Ingenuity phosphoprotein pathway analysis. Orange indicates pathways upregulated in *STK25*$^{-/-}$ cardiomyocytes while blue indicates upregulation in *STK25*$^{+/+}$. C) PKA activity in response to 10μM forskolin in *STK25*$^{+/+}$ and *STK25*$^{-/-}$ cardiomyocytes. n=3 for each condition. Mean +/- SD, *p=0.04, **p<0.01, ****p<0.0001 using ANOVA and Tukey's adjustment for multiple comparisons. D) PKA activity in response to 10μM forskolin in HEK293T cells overexpressing either empty vector, wild type STK25 or kinase-dead K49R/T174A. n=3 for each condition. Mean +/- SD, *p=0.011, **p<0.01, ****p<0.0001 using ANOVA and Tukey's adjustment for multiple comparisons.

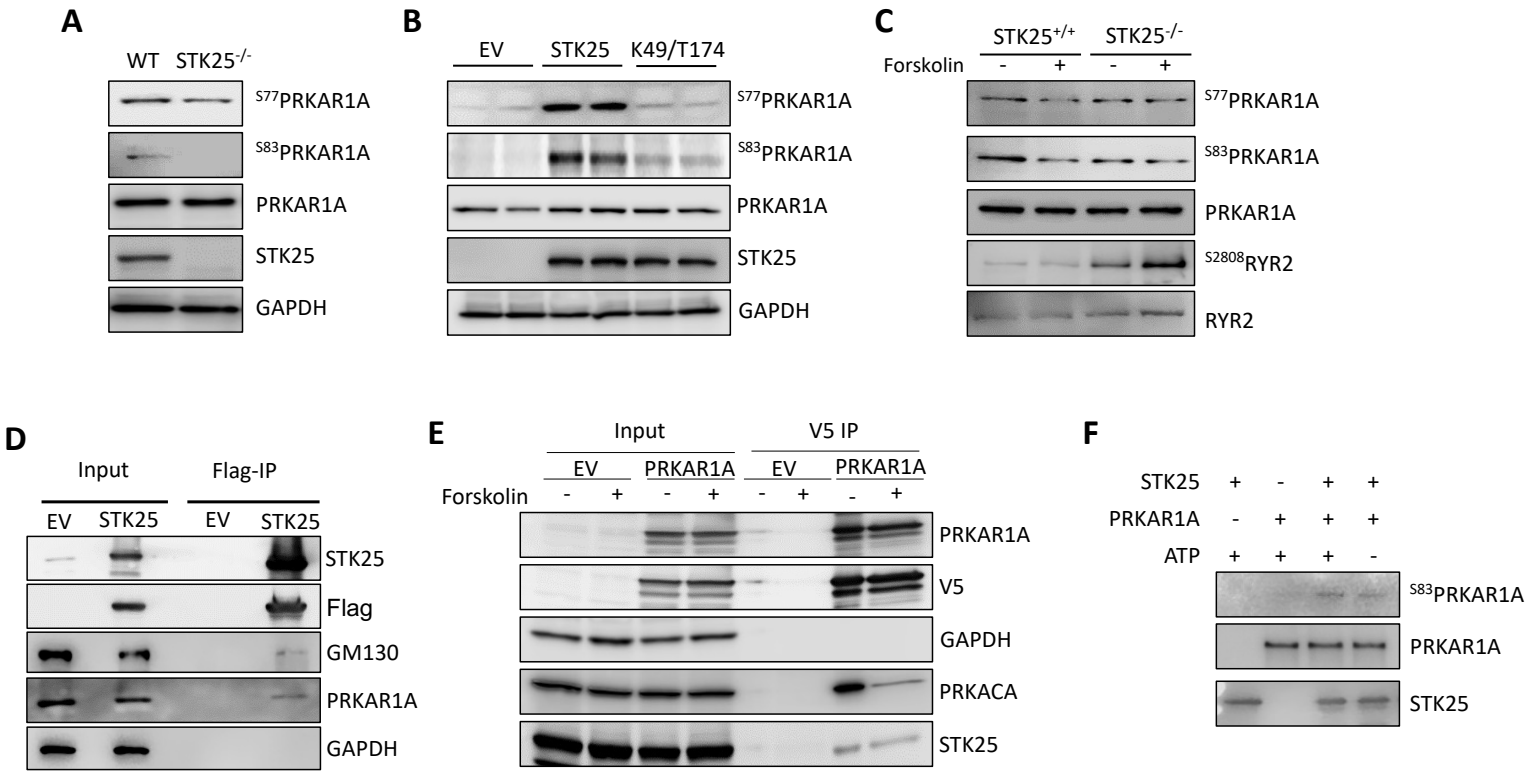

Figure 2. *STK25 binds to and phosphorylates PRKAR1A.* A) Immunoblot of PRKAR1A phosphorylation sites S77 and S83 in *STK25*$^{+/+}$ and *STK25*$^{-/-}$ cardiomyocyte protein lysates. B) Immunoblots of phosphorylation sites S77 and S83 of PRKAR1A in *STK25*$^{-/-}$ cardiomyocytes transfected with empty vector (EV), wild type STK25 and kinase dead K49R/T174A (loaded in duplicate). C) Forskolin (10μM) stimulated *STK25*$^{+/+}$ and *STK25*$^{-/-}$ cardiomyocytes immunoblotted for phosphorylation of PRKAR1A and RYR2. D) Immunoprecipitation of Flag-STK25 expressed in HEK293T cells and immunoblotted for PRKAR1A and GM130 (positive control binding partner). E) Co-immunoprecipitation of PRKAR1A-V5 with STK25 and PRKACA in HEK293T cells treated with forskolin (10μM). F) *In vitro* kinase assay of purified STK25 and PRKAR1A, immunoblotted for phosphorylation of S83 of PRKAR1A.

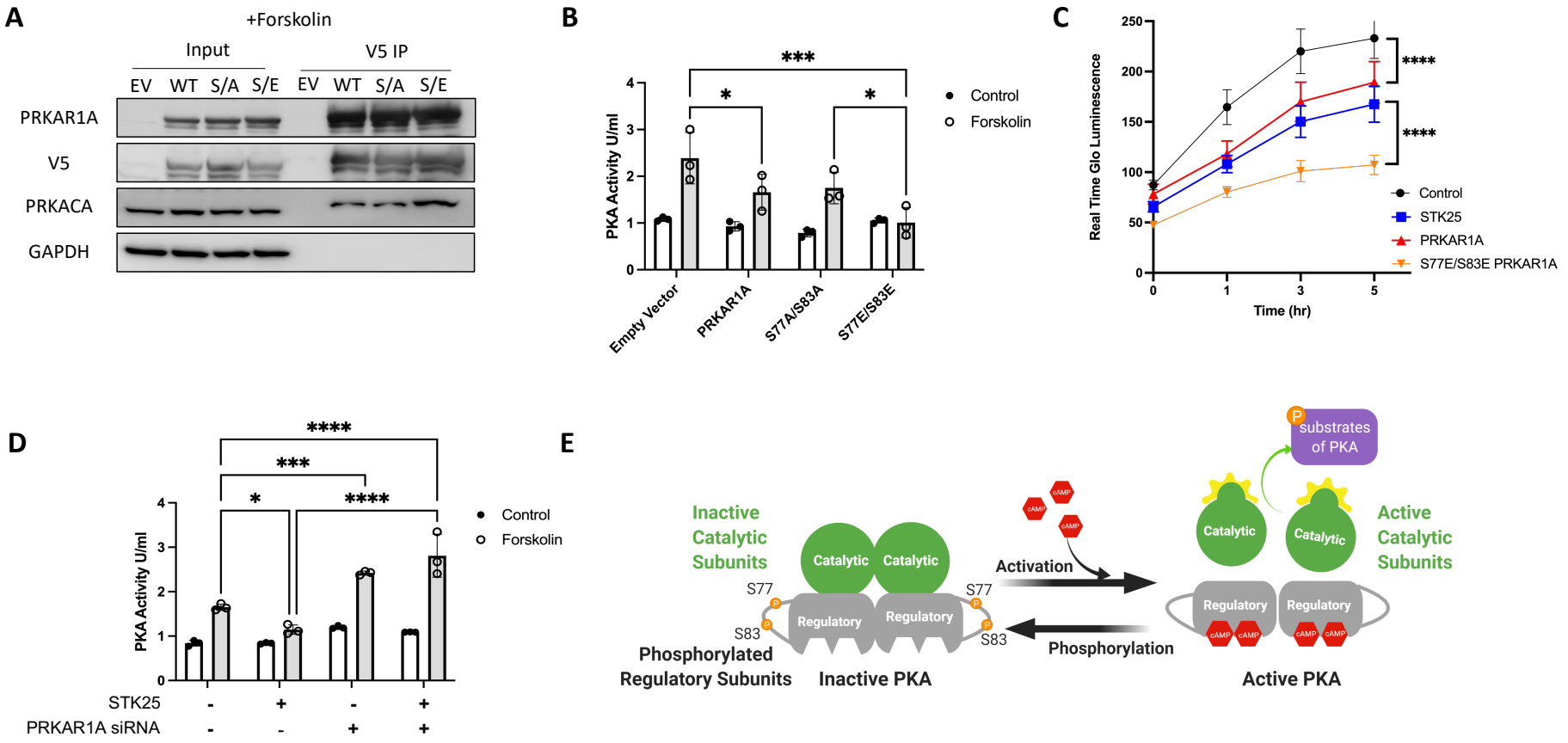

Figure 3. *Phosphorylation of PRKAR1A inhibits PKA activity.* A) Co-immunoprecipitations of V5 tagged PRKAR1A, S77A/S83A PRKAR1A or S77E/S83 PRKAR1A and immunoblotting for PRKARCA in HEK293T cells stimulated with forskolin (10μM). B) PKA activity in HEK293T cells stimulated with forskolin (10μM) and transfected with empty vector, wild type PRKAR1A, S77A/S83A PRKAR1A mutant or S77E/S83E PRKAR1A mutant as indicated. C) HEK293T cells transfected with the indicated vectors and assessed for growth by Real Time Glo for 5 hours after stimulation with forskolin (10μM). For all points in this figure, n=3 for each condition, Mean +/- SD, *p<0.05, ***p<0.001, and ****p<0.0001 by ANOVA with Tukey's adjustment for multiple comparisons. D) PKA activity in HEK293T cells stimulated with forskolin (10μM) and either overexpressing STK25 and/or the siRNA of PRKAR1A. E) Model of STK25 downregulation of the PKA pathway through phosphorylation of PRKAR1A.

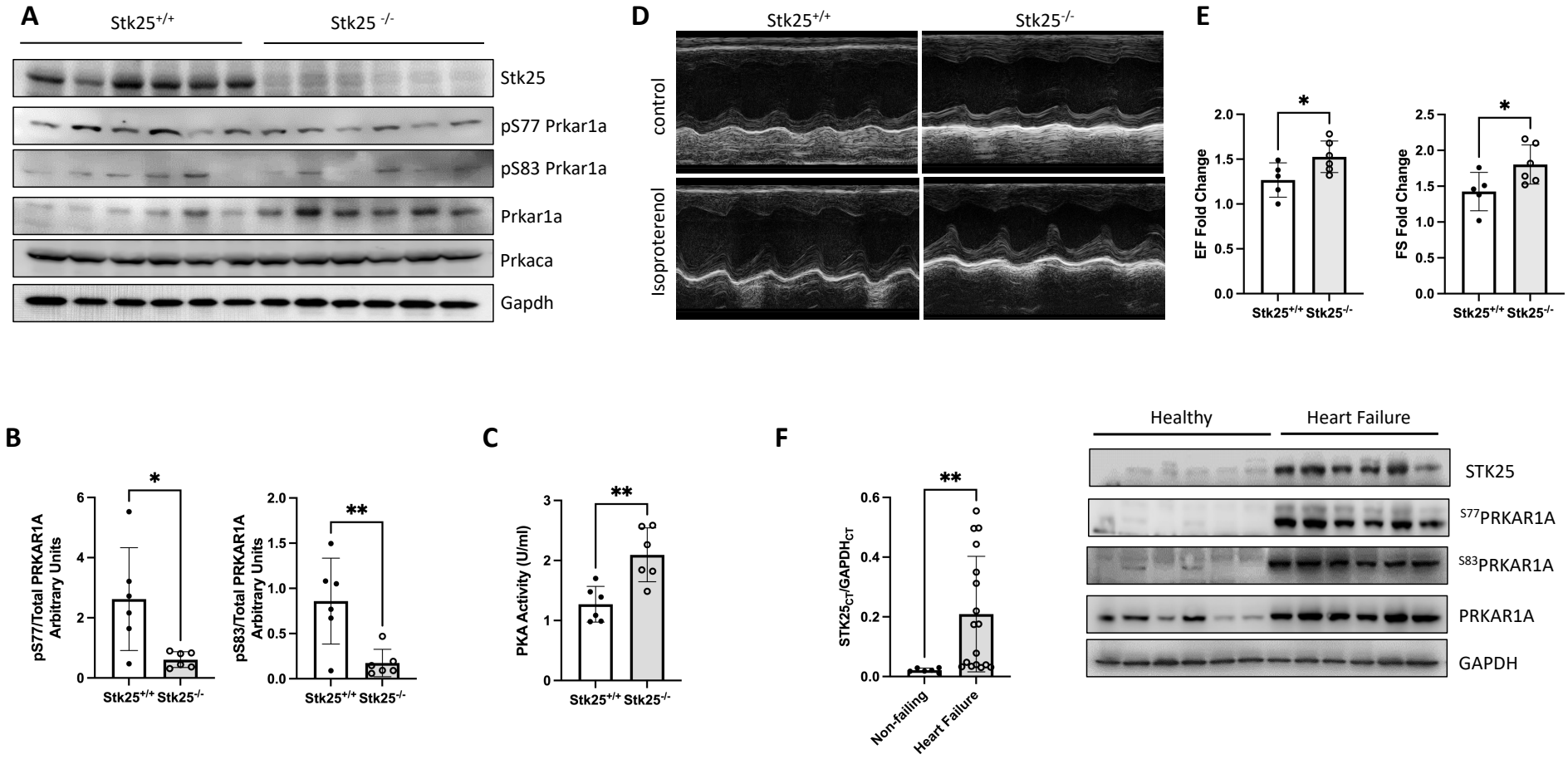

Figure 4. *Stk25 loss increases response to adrenergic stimulation in vivo.* A) Immmunoblot of Stk25, Prkaca, Gapdh, phospho-S77, phospho-S83 and total Prkar1a in *Stk25*$^{+/+}$ and *Stk25*$^{-/-}$ whole heart lysates. B) Densitometry analysis phospho-S77 and S83 relative to total Prkar1a in immunoblot shown in B. C) *Stk25*$^{+/+}$ and *Stk25*$^{-/-}$ mouse heart lysates were assessed for PKA activity *in vitro*, n=6 for each condition. D) Representative m-mode images of *Stk25*$^{+/+}$ and *Stk25*$^{-/-}$ mouse hearts stimulated with either control or isoproterenol. E) Fold change in individual heart response to isoproterenol when compared to unstimulated for ejection fraction (EF), fractional shortening (FS), n=5 for *Stk25*$^{+/+}$and n=6 for *Stk25*$^{-/-}$. F) RT-PCR (left) from left ventricular myocardium of normal hearts (n=6) or heart failure (n=17) expressed as a ratio of the threshold cycle curve (Ct) of *STK25* to *GAPDH.* Immunoblot (right) of STK25 and PRKAR1A expression and phosphorylation in protein lysates from left ventricular myocardium of normal hearts or failing hearts. N=6 for both healthy control and heart failure. Mean +/- SD, *p<0.05, **p<0.01 by student t-test in 4A and 4C and Welch's t-test in 4E and 4F.

Function		Protein Descriptions		Fold Change	Phosphorylation Sites	Protein Accessions
PKA	Regulatory subunits	PRKAR1A	cAMP-dependent protein kinase type I-alpha regulatory subunit	0.17	S77, S83	P10644
		PRKAR2A	cAMP-dependent protein kinase type II-alpha regulatory subunit	3.03	S78	P13861
	Catalytic Subunit	PRKACA	cAMP-dependent protein kinase catalytic subunit alpha	0.79	S339	P17612
PKA targets	Contractility Ca2+ handling	MYBPC	Myosin-binding protein C, cardiac-type	100.03	T498	Q14896
		Troponin	Troponin T, cardiac muscle	6.18	S132	P45379
				5.75	S285	
				5.02	S189	
		RYR2	Isoform 2 of Ryanodine receptor 2	2.51	S2808	Q92736
				2.14	S4368	
		CACNA1C	Isoform 2 of Voltage-dependent L-type calcium channel subunit alpha-1C	1.65	S1756	Q13936
	Energy Metabolism	Phosphorylase Kinase	Phosphorylase b kinase gamma catalytic chain	3.48	T325	P15735
		Glycogen Synthase	Glycogen synthase kinase-3 alpha	2.50	S21	P49840
	Gene Expression	CREB	Cyclic AMP-responsive element-binding protein 1	0.79	S271	P16220

Table 1: PKA pathway phosphoproteomic changes in STK25$^{-/-}$ compared to wild type. Fold change represents a ratio of STK25$^{-/-}$/STK25$^{+/+}$. Phosphorylation sites, description and accession numbers for each uniprot ID are listed. All changes met a significance threshold of an FDR corrected q value <0.05.

References

1. J. M. Gancedo, Biological roles of cAMP: variations on a theme in the different kingdoms of life. *Biol Rev Camb Philos Soc* **88**, 645-668 (2013).
2. S. S. Taylor, R. Ilouz, P. Zhang, A. P. Kornev, Assembly of allosteric macromolecular switches: lessons from PKA. *Nat Rev Mol Cell Biol* **13**, 646-658 (2012).
3. K. Tasken, E. M. Aandahl, Localized effects of cAMP mediated by distinct routes of protein kinase A. *Physiol Rev* **84**, 137-167 (2004).
4. M. Colledge, J. D. Scott, AKAPs: from structure to function. *Trends Cell Biol* **9**, 216-221 (1999).
5. C. Kim, C. Y. Cheng, S. A. Saldanha, S. S. Taylor, PKA-I holoenzyme structure reveals a mechanism for cAMP-dependent activation. *Cell* **130**, 1032-1043 (2007).
6. S. Barradeau, T. Imaizumi-Scherrer, M. C. Weiss, D. M. Faust, Intracellular targeting of the type-I alpha regulatory subunit of cAMP-dependent protein kinase. *Trends Cardiovasc Med* **12**, 235-241 (2002).
7. S. S. Taylor, J. A. Buechler, W. Yonemoto, cAMP-dependent protein kinase: framework for a diverse family of regulatory enzymes. *Annu Rev Biochem* **59**, 971-1005 (1990).
8. J. V. Olsen *et al.*, Global, in vivo, and site-specific phosphorylation dynamics in signaling networks. *Cell* **127**, 635-648 (2006).
9. H. Daub *et al.*, Kinase-selective enrichment enables quantitative phosphoproteomics of the kinome across the cell cycle. *Mol Cell* **31**, 438-448 (2008).
10. F. S. Oppermann *et al.*, Large-scale proteomics analysis of the human kinome. *Mol Cell Proteomics* **8**, 1751-1764 (2009).
11. J. V. Olsen *et al.*, Quantitative phosphoproteomics reveals widespread full phosphorylation site occupancy during mitosis. *Sci Signal* **3**, ra3 (2010).
12. H. Zhou *et al.*, Toward a comprehensive characterization of a human cancer cell phosphoproteome. *J Proteome Res* **12**, 260-271 (2013).
13. J. Wang, C. Gareri, H. A. Rockman, G-Protein-Coupled Receptors in Heart Disease. *Circ Res* **123**, 716-735 (2018).
14. A. R. Marks, Calcium cycling proteins and heart failure: mechanisms and therapeutics. *J Clin Invest* **123**, 46-52 (2013).
15. M. R. Bristow *et al.*, Decreased catecholamine sensitivity and beta-adrenergic-receptor density in failing human hearts. *N Engl J Med* **307**, 205-211 (1982).
16. V. Piacentino, 3rd *et al.*, Cellular basis of abnormal calcium transients of failing human ventricular myocytes. *Circ Res* **92**, 651-658 (2003).
17. C. L. Antos *et al.*, Dilated cardiomyopathy and sudden death resulting from constitutive activation of protein kinase a. *Circ Res* **89**, 997-1004 (2001).
18. S. O. Marx *et al.*, PKA phosphorylation dissociates FKBP12.6 from the calcium release channel (ryanodine receptor): defective regulation in failing hearts. *Cell* **101**, 365-376 (2000).
19. A. Kushnir, A. R. Marks, The ryanodine receptor in cardiac physiology and disease. *Adv Pharmacol* **59**, 1-30 (2010).
20. H. H. Valdivia, Ryanodine receptor phosphorylation and heart failure: phasing out S2808 and "criminalizing" S2814. *Circ Res* **110**, 1398-1402 (2012).
21. H. Zhang *et al.*, Hyperphosphorylation of the cardiac ryanodine receptor at serine 2808 is not involved in cardiac dysfunction after myocardial infarction. *Circ Res* **110**, 831-840 (2012).

22. S. Sutt *et al.*, STK25 regulates oxidative capacity and metabolic efficiency in adipose tissue. *J Endocrinol* **238**, 187-202 (2018).
23. E. Nunez-Duran *et al.*, Protein kinase STK25 aggravates the severity of non-alcoholic fatty pancreas disease in mice. *J Endocrinol* **234**, 15-27 (2017).
24. U. Chursa *et al.*, Overexpression of protein kinase STK25 in mice exacerbates ectopic lipid accumulation, mitochondrial dysfunction and insulin resistance in skeletal muscle. *Diabetologia* **60**, 553-567 (2017).
25. M. Amrutkar *et al.*, STK25 is a critical determinant in nonalcoholic steatohepatitis. *FASEB J* **30**, 3628-3643 (2016).
26. M. Amrutkar *et al.*, Protein kinase STK25 controls lipid partitioning in hepatocytes and correlates with liver fat content in humans. *Diabetologia* **59**, 341-353 (2016).
27. M. Amrutkar *et al.*, Genetic Disruption of Protein Kinase STK25 Ameliorates Metabolic Defects in a Diet-Induced Type 2 Diabetes Model. *Diabetes* **64**, 2791-2804 (2015).
28. M. Amrutkar *et al.*, Protein kinase STK25 regulates hepatic lipid partitioning and progression of liver steatosis and NASH. *FASEB J* **29**, 1564-1576 (2015).
29. E. Cansby *et al.*, Increased expression of STK25 leads to impaired glucose utilization and insulin sensitivity in mice challenged with a high-fat diet. *FASEB J* **27**, 3660-3671 (2013).
30. A. Nerstedt *et al.*, Serine/threonine protein kinase 25 (STK25): a novel negative regulator of lipid and glucose metabolism in rodent and human skeletal muscle. *Diabetologia* **55**, 1797-1807 (2012).
31. E. Cansby *et al.*, STK25 Regulates Cardiovascular Disease Progression in a Mouse Model of Hypercholesterolemia. *Arterioscler Thromb Vasc Biol* **38**, 1723-1737 (2018).
32. S. Lim *et al.*, Identification of the kinase STK25 as an upstream activator of LATS signaling. *Nat Commun* **10**, 1547 (2019).
33. S. J. Bae, L. Ni, X. Luo, STK25 suppresses Hippo signaling by regulating SAV1-STRIPAK antagonism. *Elife* **9** (2020).
34. J. Navarrete-Perea, Q. Yu, S. P. Gygi, J. A. Paulo, Streamlined Tandem Mass Tag (SL-TMT) Protocol: An Efficient Strategy for Quantitative (Phospho)proteome Profiling Using Tandem Mass Tag-Synchronous Precursor Selection-MS3. *J Proteome Res* **17**, 2226-2236 (2018).
35. X. Jiang *et al.*, Sensitive and Accurate Quantitation of Phosphopeptides Using TMT Isobaric Labeling Technique. *J Proteome Res* **16**, 4244-4252 (2017).
36. S. Tyanova *et al.*, The Perseus computational platform for comprehensive analysis of (prote)omics data. *Nat Methods* **13**, 731-740 (2016).
37. A. Subramanian *et al.*, Gene set enrichment analysis: a knowledge-based approach for interpreting genome-wide expression profiles. *Proc Natl Acad Sci U S A* **102**, 15545-15550 (2005).
38. V. K. Mootha *et al.*, PGC-1alpha-responsive genes involved in oxidative phosphorylation are coordinately downregulated in human diabetes. *Nat Genet* **34**, 267-273 (2003).
39. Y. Hayashi *et al.*, BMP-SMAD-ID promotes reprogramming to pluripotency by inhibiting p16/INK4A-dependent senescence. *Proc Natl Acad Sci U S A* **113**, 13057-13062 (2016).
40. P. W. Burridge *et al.*, Chemically defined generation of human cardiomyocytes. *Nat Methods* **11**, 855-860 (2014).

41. C. Preisinger *et al.*, YSK1 is activated by the Golgi matrix protein GM130 and plays a role in cell migration through its substrate 14-3-3zeta. *J Cell Biol* **164**, 1009-1020 (2004).
42. I. Bossis, C. A. Stratakis, Minireview: PRKAR1A: normal and abnormal functions. *Endocrinology* **145**, 5452-5458 (2004).
43. Y. Bian *et al.*, An enzyme assisted RP-RPLC approach for in-depth analysis of human liver phosphoproteome. *J Proteomics* **96**, 253-262 (2014).
44. A. Kushnir, M. J. Betzenhauser, A. R. Marks, Ryanodine receptor studies using genetically engineered mice. *FEBS Lett* **584**, 1956-1965 (2010).
45. C. J. Vlahos, S. A. McDowell, A. Clerk, Kinases as therapeutic targets for heart failure. *Nat Rev Drug Discov* **2**, 99-113 (2003).
46. A. Clerk *et al.*, Signaling pathways mediating cardiac myocyte gene expression in physiological and stress responses. *J Cell Physiol* **212**, 311-322 (2007).
47. J. Heineke, J. D. Molkentin, Regulation of cardiac hypertrophy by intracellular signalling pathways. *Nat Rev Mol Cell Biol* **7**, 589-600 (2006).
48. N. S. Dhalla, A. L. Muller, Protein Kinases as Drug Development Targets for Heart Disease Therapy. *Pharmaceuticals (Basel)* **3**, 2111-2145 (2010).
49. K. J. Haushalter *et al.*, Phosphorylation of protein kinase A (PKA) regulatory subunit RIalpha by protein kinase G (PKG) primes PKA for catalytic activity in cells. *J Biol Chem* **293**, 4411-4421 (2018).
50. R. S. Gupte, F. Traganos, Z. Darzynkiewicz, M. Y. Lee, Phosphorylation of RIalpha by cyclin-dependent kinase CDK 2/cyclin E modulates the dissociation of the RIalpha-RFC40 complex. *Cell Cycle* **5**, 653-660 (2006).
51. A. Najafi, V. Sequeira, D. W. Kuster, J. van der Velden, beta-adrenergic receptor signalling and its functional consequences in the diseased heart. *Eur J Clin Invest* **46**, 362-374 (2016).
52. M. Ungerer, M. Bohm, J. S. Elce, E. Erdmann, M. J. Lohse, Altered expression of beta-adrenergic receptor kinase and beta 1-adrenergic receptors in the failing human heart. *Circulation* **87**, 454-463 (1993).